Discovery of a series of portimine-A fatty acid esters in mussels

Vincent Hort, Sophie Bourcier

Harmful Algae 134 (2024) 102621

Contents lists available at ScienceDirect

Harmful Algae

journal homepage: www.elsevier.com/locate/hal

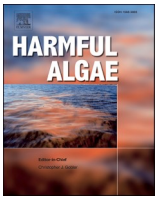

Discovery of a series of portimine-A fatty acid esters in mussels

Vincent Hort [a,*], Sophie Bourcier [b]

[a] Laboratory for Food Safety, Pesticides and Marine Biotoxins Unit, ANSES (French Agency for Food, Environmental and Occupational Health and Safety), 94701 Maisons-Alfort, France
[b] Laboratoire de Chimie Moléculaire (LCM), CNRS, Ecole Polytechnique, Institut Polytechnique de Paris, 91128 Palaiseau, France

ARTICLE INFO

Edited by Dr Po Teen Lim

Keywords:
Shellfish
Marine biotoxin fatty acid esters
Mass spectrometry
Pinnatoxins
Portimines
Vulcanodinium rugosum

ABSTRACT

Vulcanodinium rugosum is a benthic dinoflagellate known for producing pinnatoxins, pteriatoxins, portimines and kabirimine. In this study, we aimed to identify unknown analogs of these emerging toxins in mussels collected in the Ingril lagoon, France. First, untargeted data acquisitions were conducted by means of liquid chromatography coupled to hybrid quadrupole-orbitrap mass spectrometry. Data processing involved a molecular networking approach, and a workflow dedicated to the identification of biotransformed metabolites. Additionally, targeted analyses by liquid chromatography coupled to triple quadrupole mass spectrometry were also implemented to further investigate and confirm the identification of new compounds. For the first time, a series of 13-*O*-acyl esters of portimine-A ($n = 13$) were identified, with fatty acid chains ranging between C12:0 and C22:6. The profile was dominated by the palmitic acid conjugation. This discovery was supported by fractionation experiments combined with the implementation of a hydrolysis reaction, providing further evidence of the metabolite identities. Furthermore, several analogs were semi-synthesized, definitively confirming the discovery of these metabolization products. A new analog of pinnatoxin, with a molecular formula of $C_{42}H_{65}NO_9$, was also identified across the year 2018, with the highest concentration observed in August (4.5 µg/kg). The MS/MS data collected for this compound exhibited strong structural similarities with PnTX-A and PnTX-G, likely indicating a substituent $C_2H_5O_2$ in the side chain at C33. The discovery of these new analogs will contribute to deeper knowledge of the chemodiversity of toxins produced by *V. rugosum* or resulting from shellfish metabolism, thereby improving our ability to characterize the risks associated with these emerging toxins.

1. Introduction

Vulcanodinium rugosum is a benthic dinoflagellate (Nézan and Chomérat, 2011), known for producing a series of cyclic imines considered emerging marine biotoxins, such as pinnatoxins (PnTXs), pteriatoxins (PtTXs), portimines, and kabirimine. Among them, PnTXs were the first toxins identified (Chou et al., 1996b, 1996a; Selwood et al., 2014, 2010; Takada et al., 2001b, 2001a; Uemura et al., 1995; Zheng et al., 1990). Some of them are thought to result from shellfish metabolism, like PnTX-B, PnTX-C, PnTX-D, and a series of PnTX-G fatty acid esters ($n = 26$) (McCarron et al., 2012). To date, limited occurrence data are available in foodstuffs. PnTXs have been observed, with different toxin profiles, in shellfish from New Zealand, Australia, Japan, Canada, Chile, Mozambique, and several European countries, such as France, Norway, and Spain (García-Altares et al., 2014; Hess et al., 2013; Hort et al., 2023; Lamas et al., 2019; McCarron et al., 2012; McNabb et al., 2012; Norambuena and Mardones, 2023; Rambla-Alegre, 2018; Rundberget et al., 2011; Takada et al., 2001a; Tamele et al., 2022).

The PtTX group is composed of three analogs (PtTX-A, PtTX-B, and PtTX-C) that share strong structural similarities with PnTXs. All possess polyether macrocycles composed of 6,7-spiro, 5,6-bicyclo, and 6,5,6-trispiroketal rings (Fig. 1). These three PtTX analogs were exclusively isolated from the Japanese bivalve mollusc *Pteria penguin,* and have not been identified from *V. rugosum* isolates so far (Takada et al., 2001b). As a result, they likely originate from the shellfish metabolism of pinnatoxins. Recently, a compound identified from French mussels *Mytilus galloprovincialis* was putatively attributed to pteriatoxins with substantial evidence (Hort et al., 2023). Nevertheless, the lack of reference material did not allow for the definitive confirmation of this compound's identity.

Portimines and kabirimine are polycyclic ether toxins discovered over the past decade. To date, two analogs of portimines have been isolated from cultures of *V. rugosum* (Fig. 1), and their structure elucidated: portimine-A and portimine-B (Fribley et al., 2019; Selwood et al.,

* Corresponding author.
E-mail address: vincent.hort@anses.fr (V. Hort).

https://doi.org/10.1016/j.hal.2024.102621
Received 13 November 2023; Received in revised form 25 February 2024; Accepted 19 March 2024
Available online 27 March 2024

2013). Portimine-A can be produced in large quantities by Mediterranean strains of *V. rugosum* (Mondeguer et al., 2015). Despite its lower accumulation capacity compared to PnTXs, this toxin has already been detected in shellfish (Aráoz et al., 2020; Hort et al., 2023). For portimine-B, a recent study revealed the presence of a compound with the same elemental composition and strong structural similarities in mussels collected from Ingril lagoon, France. Despite the evidence provided, the lack of reference material did not enable definitive identification of portimine-B. In 2019, kabirimine was isolated from *V. rugosum* and its absolute stereochemistry was elucidated (Hermawan et al., 2019). To date, the accumulation of this metabolite has not been reported in shellfish or any other marine organism.

The acute toxicity of several *V. rugosum* metabolites has been investigated. Like for other cyclic imine toxins, PnTXs/PtTXs belong to the fast-acting toxin group (EFSA Panel on Contaminants in the Food Chain (CONTAM), 2010). Their toxicity, observed through mouse bioassays, is rapid, with neurotoxic symptoms appearing within minutes of administration, and generally leading to the mouse's death by respiratory arrest (Mondeguer et al., 2015; Munday et al., 2012; Selwood et al., 2014, 2010; Sosa et al., 2020; Takada et al., 2001b). Depending on the analog studied and route of administration, lethal dose (LD_{50}) values established vary between 13 and 2800 μg/kg. In a recent risk assessment carried out in France, a provisional acute benchmark value for PnTX-G of 0.13 μg/kg bw per day was derived from an acute oral toxicity study in mice (Arnich et al., 2020). Based on this value and a shellfish meat portion size of 400 g, a concentration lower than 23 μg PnTX/kg shellfish meat is not expected to result in adverse effects in humans. A study of the intraperitoneal toxicity of portimine-A to mice (LD_{50} = 1570 μg/kg bw) revealed much lower toxicity compared to PnTXs (Selwood et al., 2013). Furthermore, several *V. rugosum* toxins demonstrated cytotoxic and/or apoptic effects, like PnTX-G, portimine-A, and portimine-B (Clarke et al., 2021; Fribley et al., 2019). Interestingly, due to its properties, portimine-A and its congeners are the subject of a patent related to anticancer therapy (Hampton et al., 2014). Although

Pinnatoxins and pteriatoxins

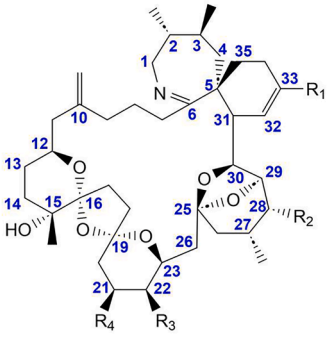

Portimine-A

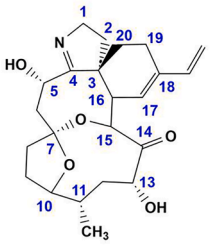

Pinnatoxin / pteriatoxin analog	Elemental composition	*m/z* MH^+	R_1	R_2	R_3	R_4
Pinnatoxin A	$C_{41}H_{61}NO_9$	712.4419		OH	H	H
Pinnatoxin B and C	$C_{42}H_{64}N_2O_9$	741.4684	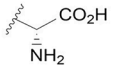	OH	H	H
Pinnatoxin D	$C_{45}H_{67}NO_{10}$	782.4837	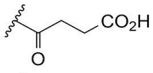	H	OH	CH_3
Pinnatoxin E	$C_{45}H_{69}NO_{19}$	784.4994	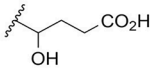	H	OH	CH_3
Pinnatoxin F	$C_{45}H_{67}NO_9$	766.4888	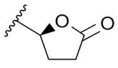	H	OH	CH_3
Pinnatoxin G	$C_{42}H_{63}NO_7$	694.4677		OH	H	H
Pinnatoxin H	$C_{43}H_{65}NO_7$	708.4833		H	OH	CH_3
28-*O*-acyl esters of pinnatoxin G	$C_{56}H_{89}NO_8$ to $C_{66}H_{99}NO_8$	904.6666 to 1034.7449		Fatty acid acyl	H	H
Pteriatoxin A	$C_{45}H_{70}N_2O_{10}S$	831.4823	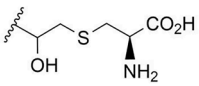	OH	H	H
Pteriatoxin B and C	$C_{45}H_{72}N_2O_{10}S$	833.4980	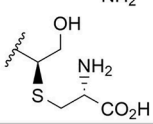	OH	H	H

Portimine-B

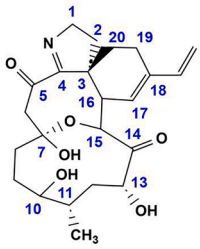

Fig. 1. Structures of pinnatoxins, pteriatoxins, and portimines.

these studies provide evidence of toxicological activity, to date, no human cases of poisoning from direct exposure in seawater or seafood consumption to PnTXs, PtTXs, portimines, or kabirimine have been confirmed. Nevertheless, acute dermatitis outbreaks involving 60 swimmers in Cuba and artisanal anglers in Senegal have recently been correlated to *V. rugosum* blooms, with the presence of portimine-A and PnTXs (Hess et al., 2022; Moreira-González et al., 2020). The causal link between these poisoning episodes, resulting from direct exposure to seawater, and these toxins is currrently under investigation.

The aim of this study was to seek unknown metabolites produced by *V. rugosum* or their biotransformed products in mussels from samples collected in Ingril lagoon, France. This locality was retained since it is considered a hotspot for the growth of this benthic dinoflagellate. To assess sample contamination, we performed untargeted acquisitions by liquid chromatography coupled to a hybrid quadrupole-orbitrap mass spectrometer (LC-MS/HRMS), complemented by the use of data processing workflows designed for the identification of unknown compounds. Additionally, liquid chromatography coupled to triple quadrupole mass spectrometry (LC-MS/MS) was also implemented. The high sensitivity level of this instrument proved particularly valuable when compounds were detected at trace levels. To secure the discovery of the new analogs discovered, various strategies were implemented, including fractionation experiments combined with chemical conversion of these compounds. After assessment of different reaction routes, semi-synthesized materials were also produced for comparison with the natural compounds. This study aimed to enhance our knowledge of the toxins produced by *V. rugosum* and their products of shellfish metabolism to provide a better overview of human exposure to these emerging toxins.

2. Materials and methods

2.1. Chemicals and reagents

All solutions were prepared using chemicals of liquid chromatography-mass spectrometry (LC-MS) grade and ultrapure water (18.2 MΩ.cm) obtained by purifying distilled water through a Milli-Q system. A PnTX-G certified reference material, concentrated to 1.92 ± 0.09 µg/mL, was purchased from NRCC (Halifax, NS, Canada). We also obtained a PnTX-A reference material, concentrated to 5.0 µg/mL, from Abraxis LLC (Warminster, PA, USA). Portimine-A (11.9 µg), Portimine-B (10 µg), PnTX-E (10.0 µg), PnTX-F (10.0 µg), and PnTX-H (10.0 µg), produced as reference materials by the Cawthron Institute (Nelson, New Zealand), were provided by Novakits (Nantes, France). Acetonitrile, methanol, acetic acid and formic acid were procured from Fisher Scientific (Loughborough, UK). Ultra-pure-grade carrier argon (Ar, 99.9999 % pure) and nitrogen (N_2, 99.999 % pure) were purchased from Linde Gas (Montereau-Fault-Yonne, France).

The protocols implemented for the synthesis of fatty acid esters of portimine-A require the use of several reagents, and in particular carboxylic acid derivatives. Myristic anhydride (purity ≥ 95.0 %) was obtained from Sigma-Aldrich® (Saint-Louis, MO, USA). Myristoyl chloride (purity ≥ 96.0 %), myristic acid (purity ≥ 98.5 %), lauric acid (purity ≥ 98.5 %), palmitic acid (purity ≥ 97.5 %), n-pentadecanoic acid (purity ≥ 98.5 %), heneicosanoic acid, (purity ≥ 98.5 %), oleic acid (purity ≥ 96.0 %), linoleic acid (purity ≥ 98.5 %), cis-4,7,10,13,16,19-docosahexaenoic acid (purity ≥ 98.5 %), stearic acid (purity ≥ 99 %), and heptadecanoic acid (purity ≥ 98 %) were purchased from Thermo Scientific Chemicals (Thermo Fisher Scientific, San Jose, CA, USA). Basic reagents were also used as catalysts. 4-(dimethylamino)pyridine (ReagentPlus®, purity ≥ 99 %), and pyridine anhydrous (purity ≥ 99,75 %) were purchased from Sigma-Aldrich®, whereas N,N'-dicyclohexylcarbodiimide (purity ≥ 98.5 %) was obtained from Thermo Scientific Chemicals.

2.2. Sampling design and sample preparation

Throughout 2018, *Mytilus galloprovincialis* mussels, which is the predominant bivalve species in this geographical area, were sampled from Ingril lagoon, situated on the Mediterranean coast of France. One kilogram of mollusks was collected monthly ($n = 12$) in parallel with the French program for monitoring emerging toxins (EMERGTOX network).

The protocol implemented for extraction of toxins from mussels and the hydrolysis reaction of extracts was similar to that described by Hort et al. (2023). For the latter, the volumes were slightly adjusted with respect to the volumetric ratio extract/NaOH 2.5 M/HCl 2.5 M (8:1:1).

An additional solid phase extraction clean-up step was also performed on the August (18 BM 161) non-hydrolyzed extract to concentrate the new PnTX analog identified in the present study. A 60 mg/3 mL Strata-X cartridge (Phenomenex; Torrance, CA, USA) was conditioned with 3 mL MeOH, followed by 3 mL 30 % MeOH. Seven milliliters of water were added to 3 mL of raw extract to be deposited. The cartridge was washed with 3 mL of a solution containing water/MeOH/NH_4OH in a ratio of 89:10:1 (v/v/v). The cartridge was dried for 3 min. The toxin was eluted with 3 mL of MeOH and collected in a clean glass tube. Before and after elution, the cartridge was dried for 3 min under reduced pressure of 10 kPa. Subsequently, the extract was evaporated to dryness under a gentle stream of N_2 at 40 °C, and 150 µL MeOH were added to the tube before vortex mixing.

2.3. Analyses by liquid chromatography coupled to mass spectrometry

2.3.1. LC-MS/HRMS analyses

The LC system used was an Ultimate 3000 (Thermo Fisher Scientific), while the detection of toxins was performed with a Q Exactive™ hybrid quadrupole-orbitrap ™ mass spectrometer (Thermo Fisher Scientific), equipped with an electrospray ionization (ESI) source using HESI-II probe (Heated). The chromatographic conditions and source parameters were similar to those described by Hort et al. (2023). Untargeted acquisitions by LC-MS/HRMS were carried out in full MS data-dependent MS^2 (full MS/dd-MS^2) mode (instrumental method A.1). For the full MS acquisition, a resolution of 70,000 full width at half maximum (FWHM), an AGC target of 3×10^6, a max IT of 100 ms, and a scan range of 100–1100 were chosen. For dd-MS^2 acquisition, the following parameter values were selected: resolution 17,500 FWHM, isolation window m/z 1.5, AGC target 5×10^4 (min AGC target of 8×10^2), and max IT 50 ms. A top N of 5 was retained with an intensity threshold of 1.6×10^4, and a dynamic exclusion of 10 s. Two normalized collision energies were chosen: 37 and 47. Two workflows were applied for data processing. The first one was based on molecular networking, a modern visualization approach to detect sets of spectra from related molecules. The other workflow was employed for detecting biotransformed metabolites from known compounds using an extensive list of 87 potential phase I and II transformations, including oxidations, reductions, hydratations, methylations, amino acid and fatty acid conjugations, and others possible transformations. For fatty acid conjugations, this list comprised 53 inputs based on the fatty acid esters previously reported for okadaic acid, dinophysistoxins, spirolides, gymnodimines, azaspiracids, and pinnatoxin-G from shellfish (Aasen et al., 2006; De la Iglesia et al., 2013; Marr et al., 1992; McCarron et al., 2012; Mudge et al., 2020). For toxin identification, the retention time (RT) should be within ± 0.1 min when a standard was available. A mass error ≤ ± 5 ppm was required for the precursor ion, and the experimental isotopic pattern had to match with the theoretical one in terms of intensity (< 25 %). An MS/MS spectrum should be acquired with the data-dependent mode, with at least six products ions and a mass error < ± 5 ppm.

Additional investigations were carried out to obtain structural information through parallel reaction monitoring (PRM) acquisitions (instrumental method A.2). An MS^2 resolution of 70,000 FWHM, an AGC target of 2×10^5, a max IT of 240 ms, an isolation window of m/z 2.0,

and max IT of 240 ms were retained. MS/MS experiments on molecular ions were also conducting, implementing a Collision-Induced Dissociation (CID) to induce in-source fragmentation. Elemental compositions of molecular ions used for structure elucidations were proposed based on the MS identification criteria previously described.

Instrument control was handled by a computer equipped with Thermo Q Exactive version 2.9 Build 2926, Xcalibur version 4.1.50 and TraceFinder™ version 4.1—EFS (Thermo Fisher Scientific). Acquired data were processed with Freestyle™ version 1.8.51.0 and Compound Discoverer 3.30.550 (Thermo Fisher Scientific).

2.3.2. LC-MS/MS analyses

When LC-MS/HRMS analyses revealed the potential presence of unknown compounds, LC-MS/MS analyses targeting these specific componds were implemented. The LC system used was a Vanquish Horizon (Thermo Fisher Scientific), while the detection of toxins was performed with a TSQ Altis triple quadrupole mass spectrometer (Thermo Fisher Scientific), equipped with an electrospray ionization source (Opta-Max NG™). The separation of toxins was performed using a Hypersil Gold (50 × 2.1 mm, 1.9 µm particle sizes, 130 Å) from Thermo Fisher Scientific. Its temperature was set to 40 °C. Eluent A consisted of water, and eluent B of acetonitrile/water at a ratio of 95:5 (v/v), with both eluents containing 50 mM formic acid and 2 mM ammonium formate. The LC flow rate was 0.400 mL/min. Two separation gradients were implemented. The gradient that provided the best chromatographic separation was programmed as follows: 50 % B held for 1.0 min, a linear gradient from 50 to 100 % B in 14 min, 100 % B held for 4.5 min, a linear gradient from 100 to 50 % B in 0.5 min, and 50 % B held for 3.0 min (instrumental method B). 2 µL were injected into the system. The mass spectrometer operated in Selected Reaction Monitoring (SRM) mode. The spray voltage was set to 500 V in positive ionization mode. The source temperature was maintained at 350 °C, and capillary temperature at 325 °C. N_2 was used as the nebulizing gas with a sheath gas pressure of 37 (arbitrary units), an auxiliary gas pressure of 6 (arbitrary units), and a sweep gas pressure of 2.9 (arbitrary units). The collision gas used was argon, with a gas pressure of 1.5 mTorr. The RF Lens voltages were set to 70 V and 105 V for quantification analyses of portimines and PnTXs respectively.

For portimines, in addition to portimine-A, 53 hypothetical fatty acid conjugates were screened (Supplementary Table 1). This list was established based on derivatives already reported for other marine biotoxins. One transition was used for quantification (Q) and two others as qualifier transitions (q). The protonated molecules were systematically chosen as precursor ions, while three specific product ions with *m/z* ratios of 384.2 (Q), 246.2 (q1), and 148.1 (q2) were retained, with respective collision energies (CE) of 22, 24, and 28 V.

For PnTXs, in addition to the known analogs (PnTX-A, PnTX-B/C, PnTX-D, PnTX-E, PnTX-F, PnTX-G, and PnTX-H), the new PnTX analog identified in the present work was included. Two transitions were selected per compound. The protonated molecules, MH^+, giving the two specific product ions with *m/z* ratios of 164.2 (Q) and 458.3 (q) were retained, with CE of 54 and 44 V, respectively. A mass resolution of 0.7 Da (full width at half maximum) was set for the first and the third quadrupoles (Q1 and Q3).

Instrument control and acquired data were managed by a computer equipped with TSQ Altis Tune Application version 3.2.2625.33, Xcalibur version 4.2.47, TraceFinder™ version 4.1 - EFS, and Freestyle™ version 1.8.51.0 (Thermo Fisher Scientific).

2.4. Isolation and hydrolysis of portimine-A fatty acid esters

A liquid chromatography fractionation combined with a hydrolysis reaction were used as a complementary approach to confirm the existence of portimine-A esters. Initially, each fatty acid ester of portimine-A detected by LC-MS/MS was isolated using instrumental method B. The non-hydrolyzed extract of the mussel sample with the highest peak intensity was selected for fractionation. For all the suspected portimine-A esters, this sample corresponded to the one collected in August (18 BM 150). Subsequently, each aliquot of the fractionated extract was hydrolyzed and analyzed to check for the disappearance of the peak corresponding to the ester and the appearance of a portimine-A peak, indicating the transformation of the ester into portimine-A.

After the LC separation, the column effluent was transferred via a divert valve (Rheodyne LLC, Rohnert Park, CA, USA) either to a glass tube (to collect the fraction) or to waste. Depending on the peak width and the chromatographic resolution between the different compounds suspected to be portimine-A esters, a fractionation window ranging between 0.2 and 0.6 min was defined. 25 µL were injected into the LC system, and the procedure was repeated up to 80 times. The fractionated extract was evaporated under an N_2 stream to achieve a volume lower than 0.2 mL. The volume was adjusted to 1 mL with MeOH. Subsequently, 0.650 mL of this fractionated extract was introduced into a vial and underwent hydrolysis, as previously described. The remaining non-hydrolyzed fractionated extract (approximately 350 µL) was kept. Both extracts were analyzed in addition to the non-fractionated extract from the same sample.

2.5. Synthesis of fatty acid esters of portimine-A

To produce fatty acid esters of portimine-A, different acylation routes were evaluated. Myristic reagents were used as a model. A detailed description of the implemented protocols is provided in Supplementary File 1. In the end, the acylation route with fatty acids using N,N'-dicyclohexylcarbodiimide (DCC) was selected and applied, with and without 4-(dimethylamino)pyridine (DMAP) catalysis, to synthesize a series of fatty acid esters of portimine-A.

Prior to use, all the glassware was heated at 150 °C in a laboratory oven for at least 2 h to elimate any residual moisture. Subsequently, the glassware was cooled, and stored in a desiccator. For all the conducted reactions, the molar ratio toxin/reagents was $\geq$ 1:10 000. An aliquot of 1 nmol of toxin in solution was taken and evaporated to dryness under a stream of N_2. Then the tube was place in a dessicator for at least 2 h. For the esterification without DMAP, 1 mL of 10 mM acid, and 0.1 mL of 100 mM DCC, both in dichloromethane, were added to dissolve the dry residue. For the esterification with DMAP, 1 mL of 10 mM acid in dichloromethane, and 0.1 mL containing 100 mM DCC and 100 mM DMAP in dichloromethane were added to dissolve the dry residue. After vortex-mixing, solutions were reacted at room temperature for 30 min for the protocol without DMAP, and for 120 min for the protocol with DMAP. Once the reaction time was completed, the solution was cooled and evaporated to dryness under a stream of N_2 at 50 °C. Finally, the dry residue was dissolved in 4.4 mL MeOH, vortex mixed, and filtered on a 0.20 µm PTFE syringe filter (Chromafil®, Macherey-Nagel GmbH & Co. KG, Düren, Germany) prior to LC-MS/MS analysis.

3. Results

3.1. Implementation of molecular networking and screening of potential phase I and II biotransformations from untargeted LC-MS/HRMS acquisitions

To investigate the existence of unknown metabolites, a molecular network was initially applied to process the data obtained through LC-MS/HRMS untargeted acquisitions (instrumental method A.1). This visualization approach allows for the detection of sets of spectra from related molecules. A second workflow dedicated to the identification of biotransformed metabolites from an original compound was also implemented. It included an extensive list of 87 phase I and II transformations with many possible combinations. The implementation of both workflows made it possible to detect a compound identified as the palmitoyl conjugate of portimine-A (palmitoyl-portimine-A or C16:0-portimine-A) in the non-hydrolyzed extract of sample 18 BM 150,

collected in July (Fig. 2). The molecular formula of the protonated molecule $MH^+$was established as $C_{39}H_{62}NO_6$ with an *m/z* ratio of 640.45703 (mass error = 0.20 ppm). As for portimine-A, no $[M+NH_4]^+$, $[M+Na]^+$ or $[M+K]^+$ adducts were observed. Even though the retention time of this portimine-A ester was unknown due to the lack of reference material, all available information pointed in the direction of a fatty acid conjugation. This peak was not detected from the hydrolyzed extract, confirming that this molecule possesses a functional group that can be hydrolyzed, like esters. The higher retention time of this analog (RT = 11.36 min) compared to portimine-A (RT = 5.34 min) highlighted its more lipophilic properties. Moreover, the MS^2 spectrum of this compound presented numerous similarities with that of portimine-A, since they shared 84 common fragments. The most intense ions of portimine-A were observed, like losses of one or two water molecules from MH^+ at *m/z* 384.2165 and at *m/z* 366.2069, the loss of CO at *m/z* 356.2215 (subsequent to a loss of water), and numerous characteristic product ions with a lower *m/z* ratio, like the ions at *m/z* 246.1488, *m/z* 148.0757, and *m/z* 134.0600.

In addition to C16:0-portimine-A, another compound with strong similarities to PnTXs was identified at a retention time of 6.16 min (Supplementary Fig. 1). This compound was detected in all samples collected in 2018, and was not detected from the quality control samples included in the same series (blank mussels and blank mussels spiked with PnTX-A, PnTX-G, and portimine-A). The molecular formula of the protonated molecule $MH^+$was established as $C_{42}H_{66}NO_9$ observed at *m/z* 728.4733 (mass error = 0.14 ppm). An MS^2 spectrum was triggered for the August sample (18 BM 161). In addition to the two water loses at *m/z* 710.4560 and *m/z* 692.4511, two characteristic product ions of pinnatoxins were observed at *m/z* 458.3269, and *m/z* 164.1434.

3.2. Confirmation of the discovery of C16:0-portimine-A and identification of other new fatty acid esters of portimine-A

3.2.1. LC-MS/MS targeted analyses

LC-MS/HRMS untargeted acquisitions provided the first evidence of the presence of C16:0-portimine-A in the July sample (18 BM 150). Considering the low peak intensity observed for this compound, and the sensitivity limitation of the instrument used, in-depth investigations were launched to try to secure the identification of this C16:0-portimine-A ester. Therefore, targeted analyses were carried out by LC-MS/MS, which offered far better sensitivity than the LC-MS/HRMS instrument. In addition, the literature indicates that for other marine biotoxins undergoing fatty acid conjugations, multiple fatty acid esters of the same toxin generally coexist in a sample. Therefore, potential other fatty acid conjugates of portimine-A were also screened by LC-MS/MS through SRM acquisition mode, with a list established based on the derivatives observed for other marine biotoxins already studied (McCarron et al., 2012; Mudge et al., 2020; Pan et al., 2022).

Since the highest portimine-A concentrations were measured between June and August, the samples collected during that period were selected, including those from May and October to consider the unknown decontamination kinetics of the potential ester forms of portimine-A. Analyses of non-hydrolyzed extracts confirmed the presence of a compound matching a palmitoyl conjugation of portimine-A and revealed the potential presence of 12 other esters of portimine-A with fatty acid chains ranging from C12 to C22. Indeed, for the three SRMs corresponding to each of these esters, peaks were systematically observed at the same retention time, with a signal-to-noise ratio higher than or equal to 3. In addition, none of them were observed in the hydrolyzed extracts of the same samples. Several functional groups other than esters such as amide, acyl chloride, nitrile, acetal, imine, and enamine can be hydrolyzed. Nevertheless, only esters, nitriles, and amides are able to undergo base-catalyzed hydrolysis, providing additional evidence of the probable identification of fatty acid esters of portimine-A. The retention time of these compounds ranged between 7.9 and 10.1 min, all higher than that of portimine-A (3.5 min), which is consistent with the more lipophilic properties of fatty acid conjugates. C16:0-portimine-A was the ester with the highest peak intensity, followed by C14:0-portimine-A, and C12:0-portimine-A (Fig. 3). The peak intensities of the other esters were lower. Interestingly, all the esters were observed in the sample collected in July (Fig. 4). Based on the SRM giving the product ion at *m/z* 384, the C16:0-portimine-A ester was predominant in that sample, with a peak intensity 13 times higher than portimine-A, whose concentration was 32.4 µg/kg (Hort et al., 2023). The C14:0-portimine-A ester followed, representing approximatively twice the peak intensity of portimine-A.

Further investigations were carried out by the establishment a correlation between the retention time and the carbon number of the fatty acid conjugates (Fig. 5). A pattern was clearly discernable, with peak retention times aligned along lines for saturated fatty acid on one side ($R^2 = 0.9998$), and fatty acids with one unsaturation on the other. For the saturated fatty acid, the distance remained approximately constant along the line between C12:0 and C18:0 (C13:0 not detected). For the monounsaturated fatty acids conjugates, the line traced from the C16:1 and the C18:1, ran parallel to the saturated line, with a slope of 1.1 in both cases. For the other unsaturated fatty acid esters ($n_{unsaturations} > 1$), the lines could not be displayed since only one analog was identified each time. Nevertheless, for all the detected C18 conjugates, the retention time decreased as the number of unsaturations increased. This pattern constituted further evidence of the first detection of portimine-A fatty acid esters.

3.2.2. Fractionation of portimine-A fatty acid esters, followed by hydrolysis reaction

To assess whether the hydrolysis of the compounds suspected to be portimine-A fatty acid esters results in the formation of portimine-A, LC fractionation experiments were first carried out to isolate the esters, and exclude portimine-A from the fractionated extracts. Nine fractions containing the 13 suspected esters of portimine-A were collected from the non-hydrolyzed extract of the July sample (18 BM 150) by implementing instrumental method B. Even though the gradient was optimized to better separate the suspected esters, it was not always possible to isolate one ester per fraction. Therefore, some fractions contained two or three compounds (Table 1). After the concentration of the fractionated extracts, an aliquot was drawn and hydrolyzed. This hydrolyzed fractionated extract was analyzed by LC-MS/MS in addition to the non-fractionated non-hydrolyzed extract, and the fractionated non-hydrolyzed extract. For each non-hydrolyzed fraction, the presence of suspected esters of portimine-A and the absence of the portimine-A were first checked and confirmed. After hydrolysis of the collected fractions, portimine-A was systematically detected, whereas the fractionated compounds no longer appeared. This experiment clearly demonstrated the transformation of the fractionated compounds into portimine-A (Table 1). When hydrolyzed, nitrile and amide functionnal groups are transformed into a carboxylic acid, whereas an ester leads to an alcohol functional group. Portimine-A does not possess any carboxylic acid functional group; therefore, the hydrolyzed compounds cannot be nitrile or amide conjugates of portimine-A.

This fractionation and hydrolysis experiment clearly provided additional evidence of the presence and existence of portimine-A esters. The results obtained for fraction #1 are illustrated in Fig. 6. Portimine-A and the suspected C12:0 portimine-A ester were detected in the non-fractionated and non-hydrolyzed extract. After fractionation, as expected, the suspected C12:0-portimine-A ester was specifically isolated. Afterwards, the extract underwent hydrolysis. Its analysis revealed the disappearance of the peak suspected to be the C12:0-portimine-A ester, with the concurrent appearance of the portimine-A peak.

3.2.3. Identification of portimine-A esters in mussels through comparison with semi-synthesized products

To definitively confirm that the compounds identified in mussels are indeed portimine-A esters, we produced semi-synthesized materials for

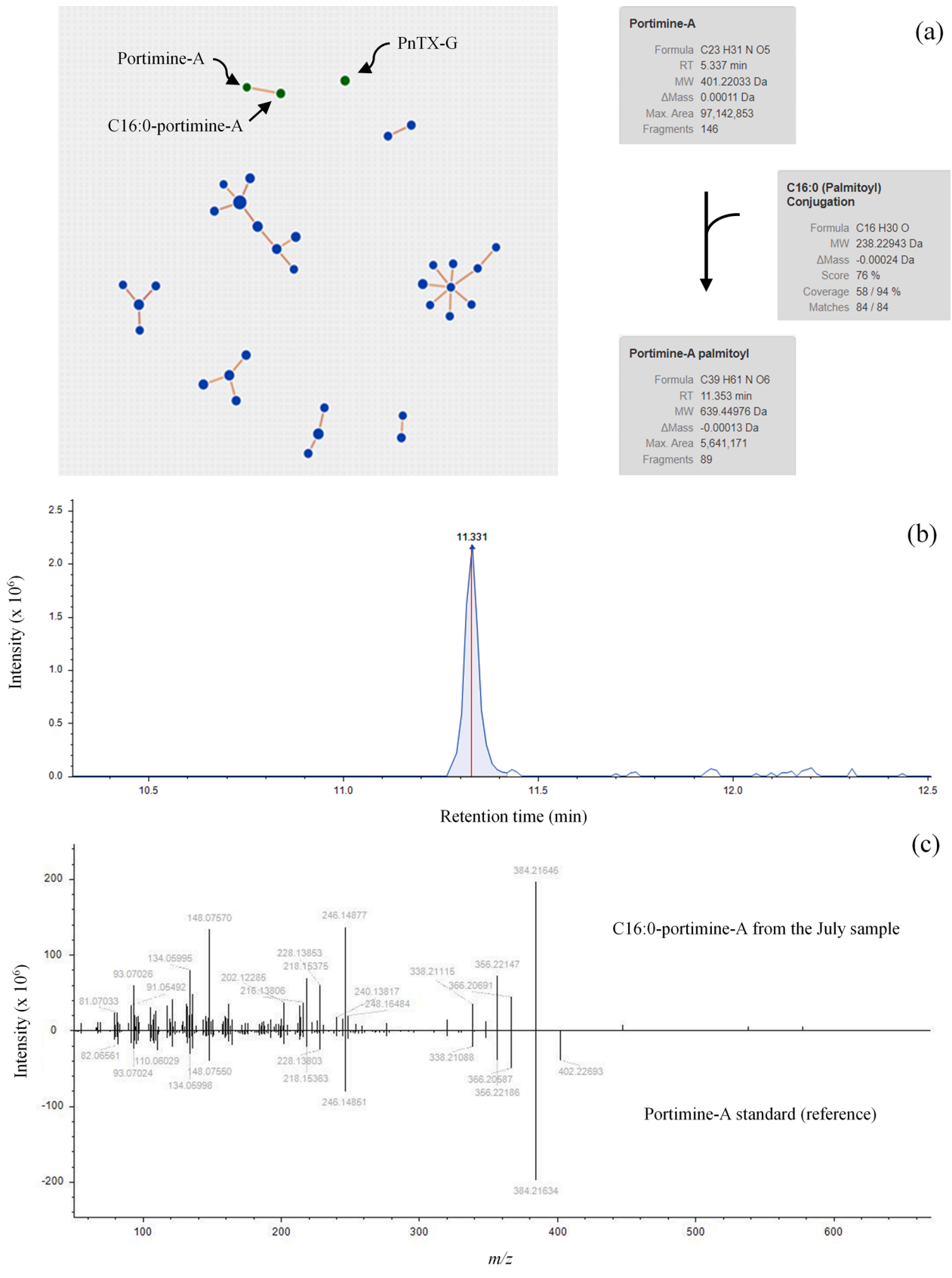

Fig. 2. Identification of C16:0-portimine-A (palmitoyl acylation) by LC-MS/HRMS in the mussel sample collected in July 2018 in Ingril lagoon, France: (a) Molecular network approach; (b) Chromatographic trace; (c) High-resolution MS/MS spectrum of the protonated C16:0 portimine A, detected in July sample (top) and of the protonated portimine-A acquired from a standard (bottom).

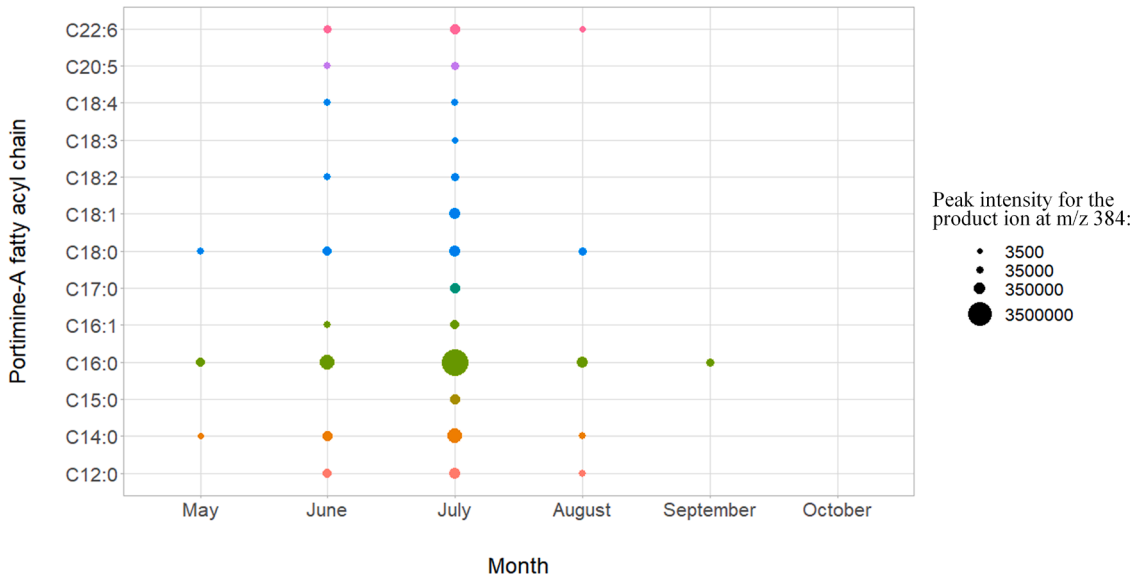

Fig. 3. Identification of portimine-A fatty acid esters by LC-MS/MS in the mussel samples collected between May and October 2018 in Ingril lagoon, France (R Core team R; Wickham et al., 2016).

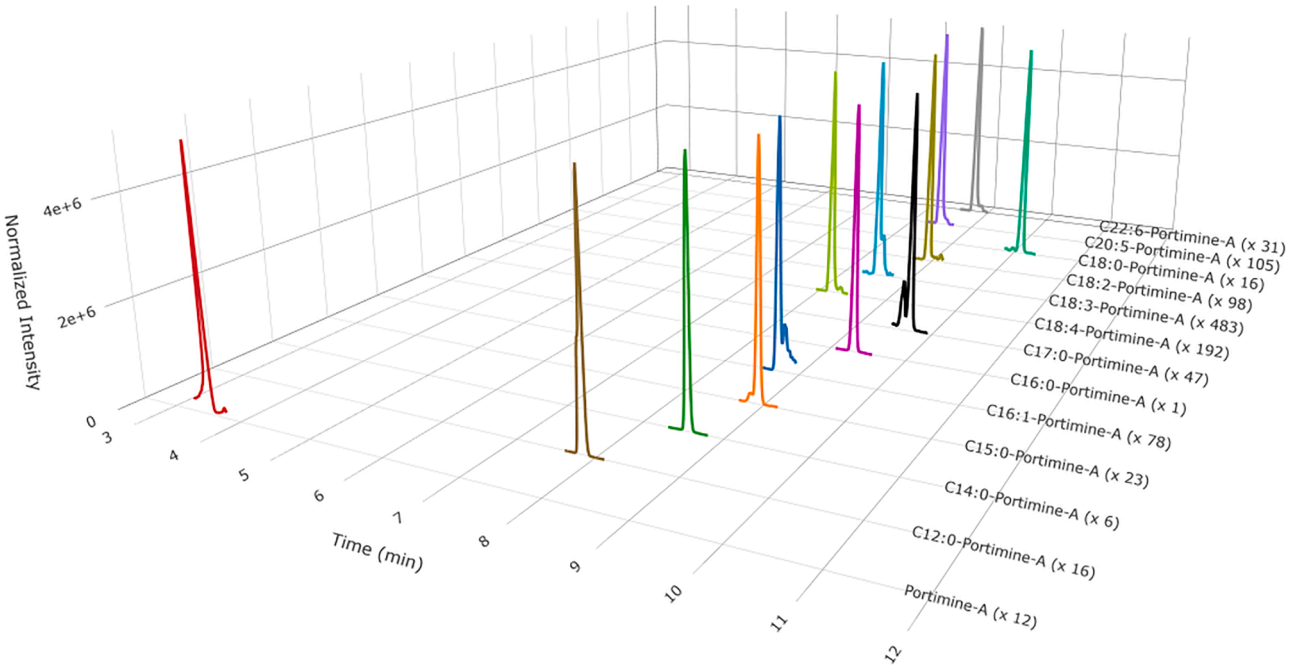

Fig. 4. LC-MS/MS detection of portimine-A and thirteen of its fatty acid esters by LC-MS/MS in the mussel sample collected in July (18 BM 150). The intensity of the peaks obtained for the quantitative transition were normalized relative to the most intense compound (C16:0-Portimine-A). The multiplicative factors are indicated in the caption. Chromatogram created with R version 4.0.3, and with the Plotly package version 4.10.0 (R Core Team, 2016; Sievert, 2020).

most of these esters. We then conducted LC-MS/MS analysis to verify if we achieved perfect matches in terms of retention time and ion ratio between the two most intense ions (*m/z* 246 and 384). Initially, different acylation routes were assessed using myristic reagents as a model. A detailed description of the results is provided in Supplementary File 1. In the end, the acylation route with fatty acids using DCC was selected and applied, with and without DMAP catalysis.

Since portimine-A has two secondary hydroxyl groups in its structure, acylation can potentially occur in both places (C5 and C13) to form the 5-*O*-myristoyl or the 13-*O*-myristoyl ester of portimine-A. For the acylation reaction with DMAP catalysis, analysis of the semi-synthesized product revealed the presence of two peaks for each three SRM traces monitored, due to the presence of both forms. The first peak (peak #1) appeared at 8.3 min, whereas the second (peak #2) was observed at 9.2 min (Supplementary Data File 1). It is important to note that the suspected C14:0-portimine-A ester detected in the mussel extracts had the same retention time as peak #1 observed from the semi-synthesized product. Based on these results, it was also decided to include three SRM traces corresponding to the portimine-A doubly acylated in the method to check if 5,13-di-*O*-myristoyl-portimine-A was also synthesized. The precursor ion retained was the protonated compound MH^+ at *m/z* 1132.84, whereas the three characteristic product ions of portimine-A at *m/z* 384, 246, and 148 were selected, as for the single acylation of the toxin. The chromatogram showed a peak corresponding

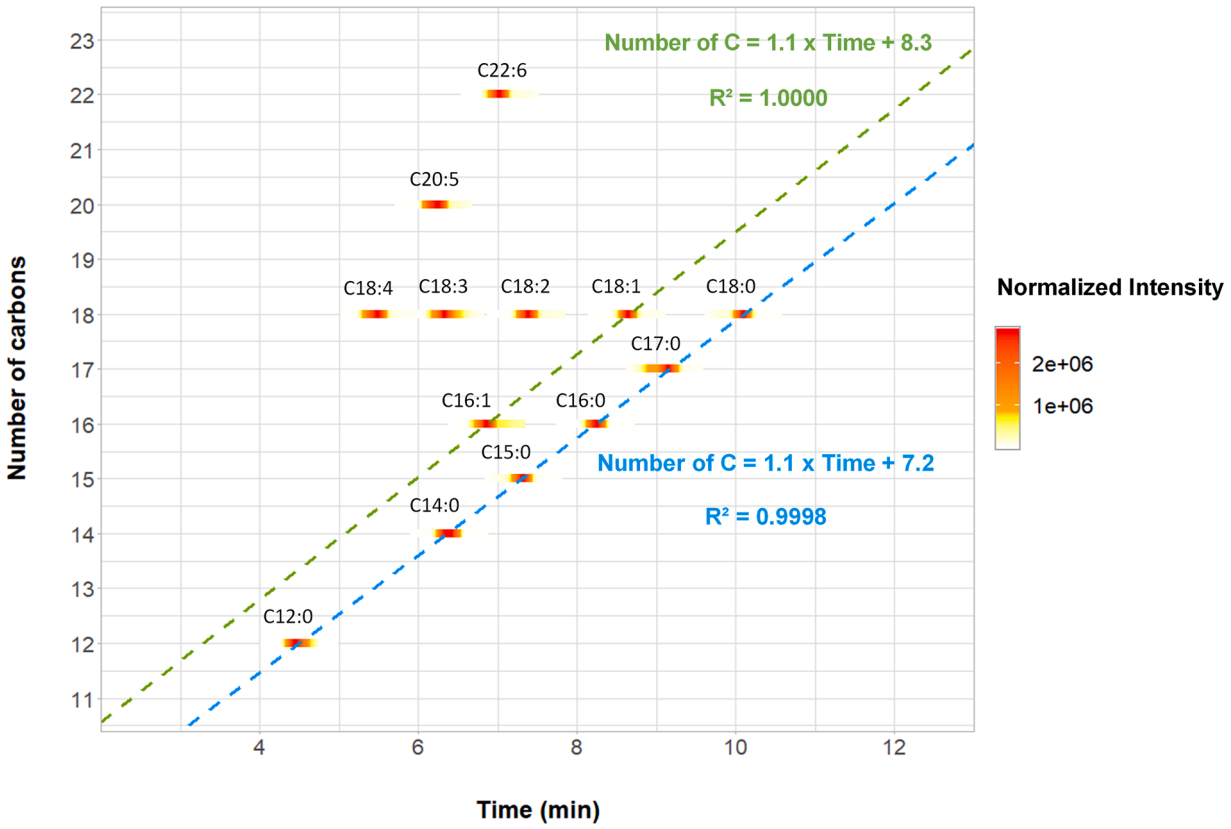

Fig. 5. Correlation between the retention times of the thirteen suspected portimine-A esters and the structure of their fatty acid chain. (a) Linear regression for saturated fatty acid esters (blue dotted line). (b) Linear regression for monounsaturated esters (green dotted line).

Table 1
Detection of portimine-A and its esters in each fraction collected from the sample collected in July (18 BM 150).

Fraction	Fractionation window (min)	Suspected ester collected	LC-MS/MS		
			Portimine-A esters		Portimine-A
			Non-hydrolyzed extract	Hydrolyzed extract	Hydrolyzed extract
#1	4.35 – 4.65	C12:0	Detected	Not detected	Detected
#2	5.20 – 5.80	C18:4	Detected	Not detected	Detected
#3	6.10 – 6.60	C14:0; C18:3; C20:5	Detected	Not detected	Detected
#4	6.72 – 7.18	C16:1; C22:6	Detected	Not detected	Detected
#5	7.20 – 7.60	C15:0; C18:2	Detected	Not detected	Detected
#6	8.05 – 8.45	C16:0	Detected	Not detected	Detected
#7	8.53 – 8.80	C18:1	Detected	Not detected	Detected
#8	8.80 – 9.3	C17:0	Detected	Not detected	Detected
#9	9.95 – 10.30	C18:0	Detected	Not detected	Detected

to this compound at a retention time of 14.3 min (Supplementary File 1). Based on these results, we assume that both hydroxyl groups can undergo individual or simultaneous conjugation during synthesis with DMAP, resulting in 5-O-acyl, 13-O-acyl, and 5,13-di-O-acyl esters of portimine-A.

For acylation with DCC used alone (without DMAP), the first peak at 6.6 min (peak #1) was observed alone, neither the peak #2 nor the peak corresponding to 5,13-di-*O*-myristoyl-portimine-A were detected. In addition the reaction was almost total since the peak of portimine was observed at trace level (Supplementary Data File 1). Therefore, to confirm the discovery of the series of fatty acid conjugates of portimine-A in the samples analyzed, this acylation route was retained to produce the desired acylated products from the different carboxylic acids purchased. In addition to C14:0-portimine-A ester, C12:0-portimine-A (dodecanoyl-portimine-A), C15:0-portimine-A (n-pentadecanoyl-portimine-A), C16:0-portimine-A (hexadecanoyl-portimine-A), C17:0-portimine-A (heptadecanoyl-portimine-A), C18:0-portimine-A (octadecanoyl-portimine-A), C18:1-portimine-A ((Z)-octadec-9-enoyl-portimine-A), C18:2-portimine-A ((9Z,12Z)-octadeca-9,12-dienoyl-portimine-A) and C22:6-portimine-A (heneicosanoyl-portimine-A) esters were produced.

The semi-synthesized materials were injected in a same batch with the non-hydrolyzed extracts of mussels. C16:1, C18:3, C18:4, and C20:5-portimine-A were not prepared, because they were not easily commercially available. The results showed a perfect retention time match (Supplementary Table 2). For instance, the maximum retention time difference between the standard and the extract of sample 18 BM 150 was 0.02 min for C12:0-portimine-A. The compliance of the ion ratio was also checked. The maximum relative deviation was 15.9% for C18:0, clearly lower than the guideline values used for the identification of pesticides or pharmacologically active residues (± 30% and ± 40%, respectively). For the four fatty acid esters of portimine-A that were not synthesized, the ion ratios obtained from the mussel extracts were compared with the values of the nine reference material produced. The

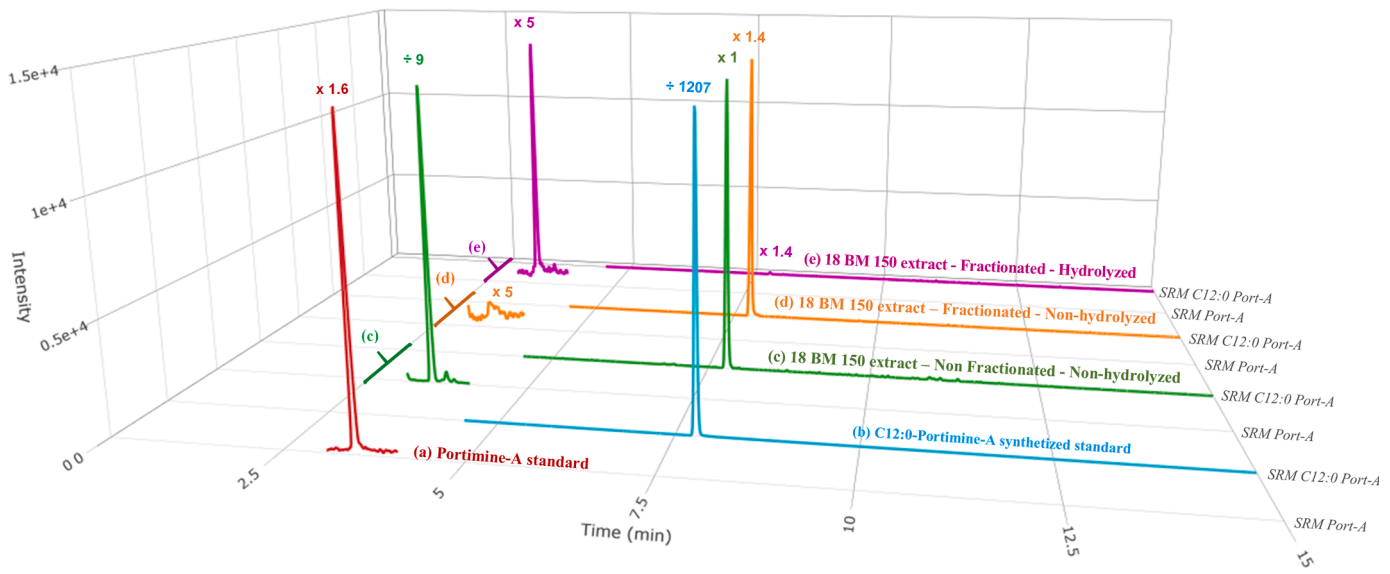

Fig. 6. LC-MS/MS investigations carried out for the C12:0-portimine-A ester performed using a fractionation approach combined with hydrolysis treatment (c, d, e), and comparison with the portimine-A standard (a) and the semi-synthesized product of the C12:0-portimine-A ester (b). SRM Port-A and SRM C12:0 Port-A correspond to the quantitative transitions of portimine-A or C12:0-portimine-A ester, respectively. The multiplication or division factors, applied to the original intensity of the peaks, are indicated above the peaks. This graph was created with R version 4.0.3, and with the Plotly package version 4.10.0 (R Core Team, 2016; Sievert, 2020).

ion ratios for the latter were similar and fell within the range of 4.5% and 6.6%, whereas for C16:1, C18:3, C18:4, and C20:5 detected in the sample, the ion ratios were 5.9, 5.4, 5.6 and 4.6%, respectively. Therefore, the ion ratios of theses non-synthesized esters were also in agreement with those of the reference materials produced. This comparison with synthesized products left no doubt about the identification of these 13 esters in mussel samples.

The DCC acylation of portimine-A with DMAP catalysis was also implemented with all the carboxylic acids to carefully check the absence of the acylated forms in the mussel extracts corresponding to the acylation of the other hydroxyl of portimine-A (peak #2), and to portimine-A doubly acylated with the same fatty acid chain on both hydroxyls. LC-MS/MS analyses were carried out. For portimine-A doubly acylated, the SRMs corresponded to the theoretical MH^+ precursor ion giving the characteristic product ions of portimine-A at *m/z* 148.07, 246.13, 384.21. As for the DCC acylation without DMAP, nine standards were synthesized from C12:0, C14:0, C15:0, C16:0, C17:0, C18:0, C18:1, C18:2, and C22:6 fatty acids. The synthetic products and the mussel extracts were analyzed. Results of analyses confirmed the exclusive presence of the ester forms corresponding to peak #1 in the mussel samples, as peak #2 and the peak corresponding to the doubly acylated portimine-A were never observed.

3.2.4. *Structural elucidation of fatty acid esters of portimine-A*

The semi-synthesized products obtained through DMAP catalysis have revealed the presence of 5-*O*-acyl, 13-*O*-acyl, and 5,13-di-*O*-acyl esters of portimine-A. However, only one of these forms seems to be favored naturally, and appears to be accessible for enzymatic acylation, as a single peak was observed in mussels corresponding to either a fatty acid conjugation on the C5 or C13. To identify this conjugation site, a study of the fragmentation of molecular ions of portimine-A (PAH^+), and portimine-B (PBH^+) was conducted through MS/MS experiments (Supplementary Table 3). The data collected have been summarized on Fig. 7, unveiling a common fragmentation pattern for both protonated analogs. In this fragmentation scheme, we can see that most of the ions obtained on the CID mass spectrum of PAH^+ are shifted by 16 amu. on that of PBH^+, corresponding to the presence of an additional oxygen atom in the portimine B structure. For both compounds, the fragmentation of MH^+ starts with the loss of one water molecule. Then, this fragment ion loses consecutively CO and/or one or two H_2O molecules. Given the similar fragmentation patterns, the loss of water molecule from MH^+ implies a protonated form on hydroxyl carried by C13, common to both portimines. Subsequently, the MS^2 spectra of the two protonated C14:0-portimine-A esters (C14:0-PAH^+) acquired from the reference materials were studied. For peak #1, the molecular ion of the ester was not observed, whereas for peak #2, ions at *m/z* 612.4249 $[C14:0\text{-}PAH]^+$, 594.4146 $[C14:0\text{-}PAH—H_2O]^+$, 576.4039 $[C14:0\text{-}PAH\text{-}2H_2O]^+$, and *m/z* 566.4197 $[C14:0\text{-}PAH—H_2O—CO]^+$ were detected (Supplementary Fig. 2). This indicates that the ester is located on the hydroxy group at C5, which is not involved in the elimination of the first water molecule from the molecular ion. Consequently, the compound obtained at the first retention time, corresponding to the natural compounds, is the 13-*O*-acyl ester of portimine-A. The protonated molecule on the ester's oxygen loses the corresponding fatty acid in the first fragmentation, explaining why the molecular ion is not observed. The structures of the 13 fatty acid esters are presented in Fig. 8.

3.3. *Confirmation of the discovery of a new pinnatoxin analog*

3.3.1. *Structural information*

The implementation of the workflow dedicated to the identification of biotransformed metabolites made it possible to identify a compound suspected to be a new PnTX analog. To delve deeper, additional LC-MS/HRMS acquisitions were initiated to obtain more comprehensive high-resolution MS/MS spectra. Mussels collected in August (18 BM 161) were selected since the highest peak intensity was observed in that sample. To obtain an enriched spectrum, the extract was concentrated 20 times through SPE cleanup, and PRM acquisitions were carried out (instrumental method A.2). The precursor ion at *m/z* 728.4738 was selected and fragmented. The MS^2 spectrum obtained for this compound, observed at a retention time of 5.9 min, showed strong similarities with PnTXs (Fig. 9). In the *m/z* range of 100 to 573, no fewer than 89 product ions were shared with PnTX-G, with *m/z* differences systematically $\leq$ 2 ppm. Moreover, the MS^2 profile distributions of both compounds were very similar. In addition to the precursor ion at *m/z* 728.4718, we observed a series of water losses at *m/z* 710.4614 $[MH\text{-}H_2O]^+$, 692.4509 $[MH\text{-}2H_2O]^+$ and *m/z* 674.4405 $[MH\text{-}3H_2O]^+$. The same number of water losses from the protonated PnTX-G was observed

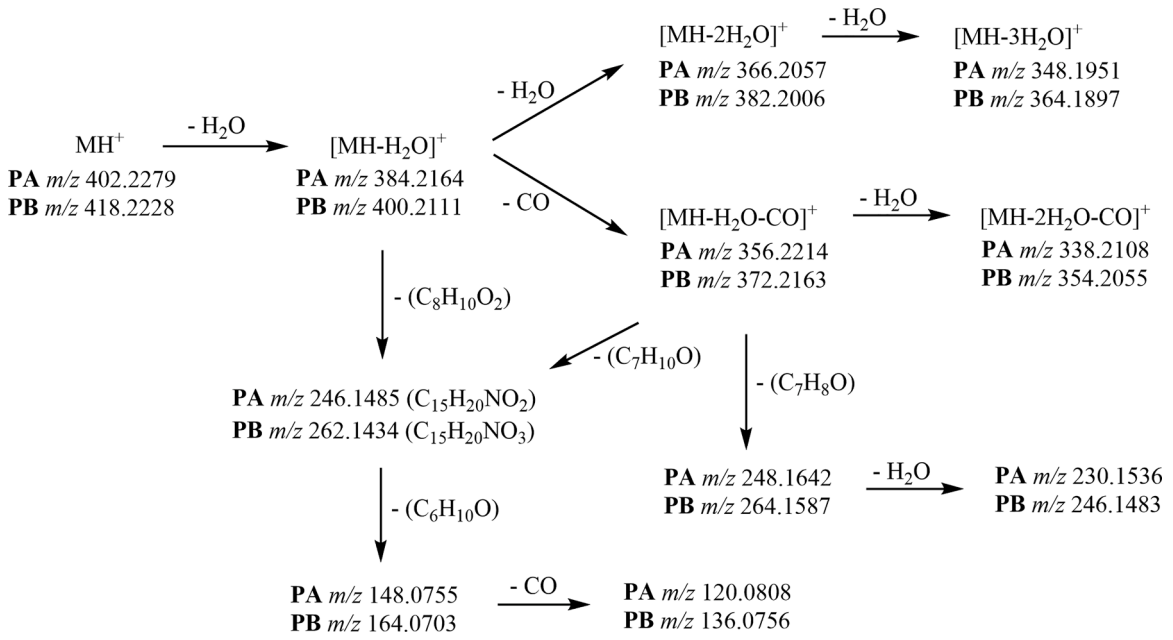

Fig. 7. Decomposition pathways of molecular ions of Portimines A (PA, $C_{23}H_{31}O_5N$) and B (PB, $C_{23}H_{31}O_6N$) obtained by ESI-Pos-MS/HRMS.

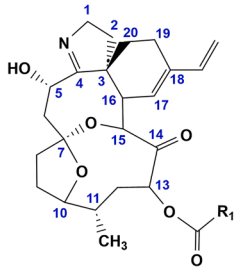

Analog	R_1	Molecular formula	Monoisotopic mass (Da)
C12:0 portimine-A	$C_{11}H_{23}$	$C_{35}H_{53}NO_6$	583.3872
C14:0 portimine-A	$C_{13}H_{27}$	$C_{37}H_{57}NO_6$	611.4185
C15:0 portimine-A	$C_{14}H_{29}$	$C_{38}H_{59}NO_6$	625.4342
C16:0 portimine-A	$C_{15}H_{31}$	$C_{39}H_{61}NO_6$	639.4498
C16:1 portimine-A	$C_{15}H_{29}$	$C_{39}H_{59}NO_6$	637.4342
C17:0 portimine-A	$C_{16}H_{33}$	$C_{40}H_{63}NO_6$	653.4655
C18:0 portimine-A	$C_{17}H_{35}$	$C_{41}H_{65}NO_6$	667.4811
C18:1 portimine-A	$C_{17}H_{33}$	$C_{41}H_{63}NO_6$	665.4655
C18:2 portimine-A	$C_{17}H_{31}$	$C_{41}H_{61}NO_6$	663.4498
C18:3 portimine-A	$C_{17}H_{29}$	$C_{41}H_{59}NO_6$	661.4342
C18:4 portimine-A	$C_{17}H_{27}$	$C_{41}H_{57}NO_6$	659.4185
C20:5 portimine-A	$C_{19}H_{29}$	$C_{43}H_{59}NO_6$	685.4342
C22:6 portimine-A	$C_{21}H_{31}$	$C_{45}H_{61}NO_6$	711.4498

Fig. 8. Structure of the 13 fatty acid esters of portimine-A.

($n = 3$). The elemental compositions of the principal product ions are presented in Table 2.

On the basis of the MH^+ fragmentation scheme following retro Diels-Alder reaction of PnTXs described by Selwood et al. (2010), we can assume that the structure of the new PnTX analog is closely related to PnTX-A and PnTX-G, with a likely different R_1 substituent in the side chain at C33 (Fig. 1). Like PnTX-A and PnTX-G, its radical R_4 certainly corresponds to a hydrogen atom, as we observed product ions specific to PnTX-A and PnTX-G at *m/z* 432, *m/z* 414, and *m/z* 396 (Fig. 10). Conversly, the product ions specific to PnTX-E and PnTX-F ($R_4 = CH_3$) at *m/z* 446, *m/z* 428, and *m/z* 410 were not identified. The radical R_3 is likely a hydrogen atom, as the products ions at *m/z* 458, *m/z* 440, and *m/z* 422 are detected, while product ions of PnTX-E and PnTX-F at *m/z* 488, *m/z* 476, *m/z* 470, *m/z* 452, and *m/z* 434, characteristics of a hydroxyl group, were not detected. Therefore, the product ion at *m/z* 572 probably has the same structure and elemental composition as the corresponding ion obtained from the protonated PnTX-A and PnTX-G. These results allow to determine the elemental composition of the radical R_1: $C_2H_5O_2$ (Fig. 10). In the scenario where this compound arises from the biotransformation of a known pinnatoxin, our workflow used for identifying biotransformed metabolites from an original compound indicates that this analog could potentially be either a reduced and methylated form of PnTX-A, or a hydratated and oxidized form of PnTX-G. However, it is important to note that this hypothesis does not provide certainty regarding whether this PnTX analog indeed results from the metabolization of PnTX-A or PnTX-G.

3.3.2. *LC-MS/MS indirect quantitation of the new analog of PNTX*

The new analog of PnTXs was detected and quantified by LC-MS/MS through SRM scans. In the absence of reference material, indirect quantification was performed using the PnTX-G calibration curve. The precursor ion at *m/z* 728.5 was selected, fragmented, and the product ions at *m/z* 164.2 and 458.4 were recorded. As previously observed through LC-MS/HRMS analysis, a chromatographic peak at 4.2 min was consistently detected in all the samples collected in 2018 in Ingril lagoon, France, for both transitions. This compound was the first to elute among all the screened PnTX analogs, with retention times ranked as follows: new PnTX analog < PnTX-A < PnTX-E < PnTX-F < PnTX-G < PnTX-H. The concentrations measured ranged between 0.4 and 4.5 µg/kg, with the highest value observed in August (Table 3). The ion ratio *m/z* 458.3/164.2 calculated from this sample was 39 %. This compound resisted hydrolysis.

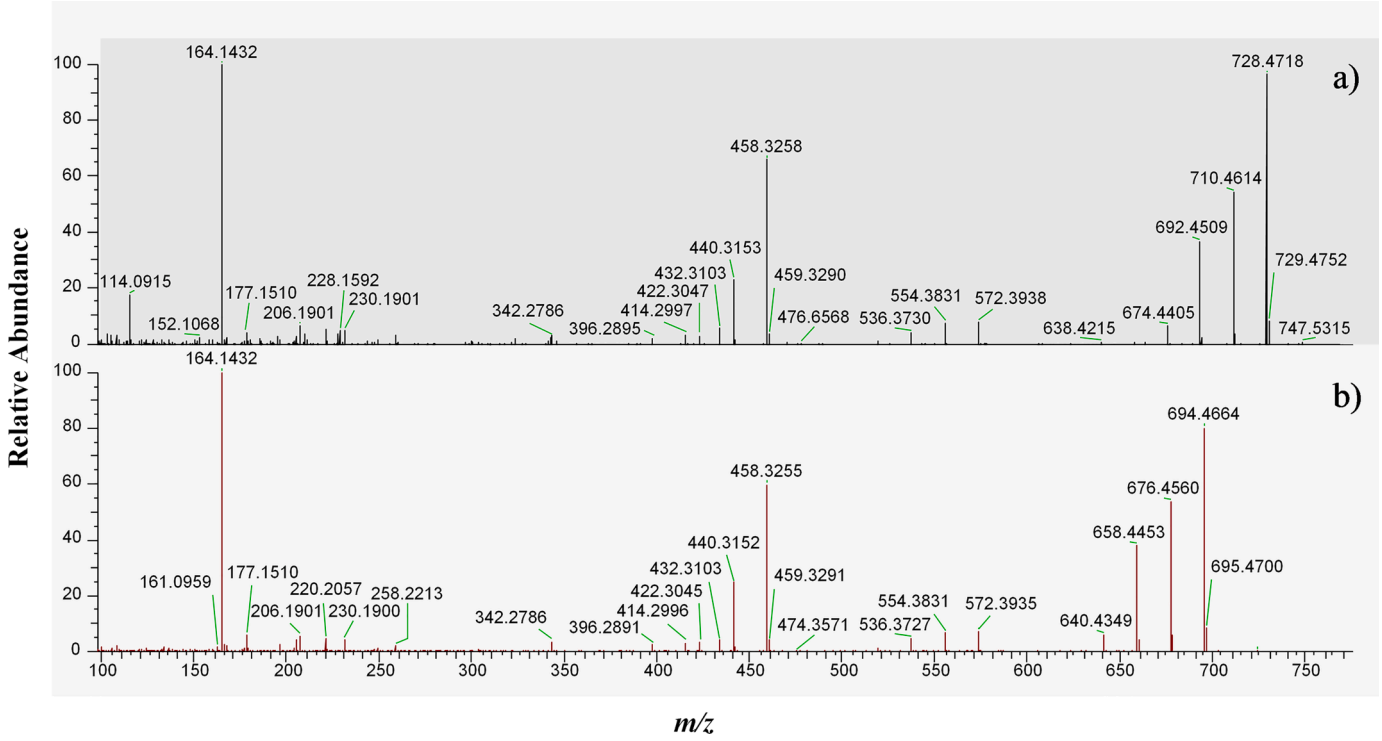

Fig. 9. HR-MS/MS spectra of molecular ions obtained from concentrated extract of July sample (18 BM 161). (a) Precursor ion at *m/z* 728.4718 corresponding to an elemental composition $C_{42}H_{66}NO_9$. (b) Protonated molecule of PnTX-G.

Table 2
Fragmentation of the precursor ion at *m/z* 728.4738 for the sample collected in August (18 BM 161), and elemental composition of the principal product ions.

m/z	Elemental composition	Δ ppm
164.1432	$[C_{11}H_{18}N]^+$	−0.96
204.1746	$[C_{14}H_{22}N]^+$	−0.6
206.1901	$[C_{14}H_{24}N]^+$	−1.32
220.2056	$[C_{15}H_{26}N]^+$	−1.62
230.1901	$[C_{16}H_{24}N]^+$	−1.17
248.2005	$[C_{16}H_{26}NO]^+$	−1.48
342.2790	$[C_{23}H_{26}NO]^+$	−0.53
396.2891	$[C_{26}H_{38}NO_2]^+$	−1.61
414.2997	$[C_{26}H_{40}NO_3]$	−1.40
422.3047	$[C_{28}H_{40}NO_2]^+$	−1.46
432.3103	$[C_{26}H_{42}NO_4]+$	−1.35
440.3153	$[C_{28}H_{42}NO_3]^+$	−1.42
458.3258	$[C_{28}H_{44}NO_4]^+$	−1.50
536.3730	$[C_{34}H_{50}NO_4]^+$	−0.74
554.3831	$[C_{34}H_{52}NO_5]^+$	−1.65
572.3938	$[C_{34}H_{54}NO_6]^+$	−1.42
674.4405	$[C_{42}H_{60}NO_6]^+$	−1.50
692.4509	$[C_{42}H_{62}NO_7]$	−1.71
710.4614	$[C_{42}H_{64}NO_8]^+$	−1.72
728.4718	MH^+; $[C_{42}H_{66}NO_9]^+$	−1.97

4. Discussion

LC-MS/HRMS was implemented to try to identify unknown metabolites associated with *V. rugosum*. The implementation of a molecular networking approach and a workflow dedicated to the study of biotransformation led to the detection of a first portimine-A fatty acid ester in the July sample (18 BM 150). All available information pointed towards a palmitoyl conjugate of portimine-A, including the elemental composition and the MS/MS spectra similarities. The detection of this fatty acid ester with a low intensity prompted further investigations to aim to identify additional fatty acid esters of portimine-A. The use of an LC-MS/MS instrument with highest sensitivity made it possible to identify 12 other fatty acid ester candidates of portimine-A, with carbon chain ranging from C12 to C22. These results were unequivocally confirmed by examining the correlation between the retention time of the compounds and their fatty acid chain, conducting the collection of fractions containing the esters followed by hydrolysis treatment, and performing the semi-synthesis of nine fatty acid esters of portimine-A. Among the samples collected in 2018, July sample exhibited the largest chemodiversity, as all the esters discovered in this study were detected. As shown in a study carried out with the same samples analyzed over 2018, the portimine-A concentration measured for this July sample after hydrolysis of the extract was almost two times higher than without treatment, with 32.4 and 59.4 μg/kg, respectively (Hort et al., 2023). In addition, this sample displayed the largest difference between both results (Δ = 27.0 μg/kg). Therefore, it was not surprising to detect all the esters discovered in that sample. It should also be noted that the C16:0 portimine-A ester exhibited the highest peak intensity detected by LC-MS/MS, likely explaining why this ester was the only one detected by LC-MS/HRMS among the 13 identified, as this instrument is known to be less sensitive. In a mussel composition study of the species *Mytilus galloprovincialis* from the Black Sea, C16:0, C22:6, C20:5, and C16:1 were the predominant fatty acids observed among the 27 screened (Dernekbasi et al., 2015). It is worth noting that in the present study, these four fatty acids were implicated in the formation of portimine-A fatty acid esters. Moreover, with the exception of C12:0 (not followed in the composition study), all the fatty acids conjugated to portimine-A were reported in the composition of mussels. A similar observation was made in a previous study targeting PnTX-G esters (Hort et al., 2023).

The toxicity of portimine-A esters has not been studied. For okadaic acid, dinophysistoxins, and PnTX-G, their fatty acid conjugated forms are generally considered less potent than their parent toxin (Aráoz et al., 2020; Yanagi et al., 1989). Nevertheless, the fatty acid conjugated forms can be hydrolyzed by lipases and other enzymes to release free-form toxins into the gastrointestinal tract during human digestion (Braga et al., 2016; Manita et al., 2017). In Chile, 26 individuals experienced a massive intoxication episode after consuming mussels contaminated

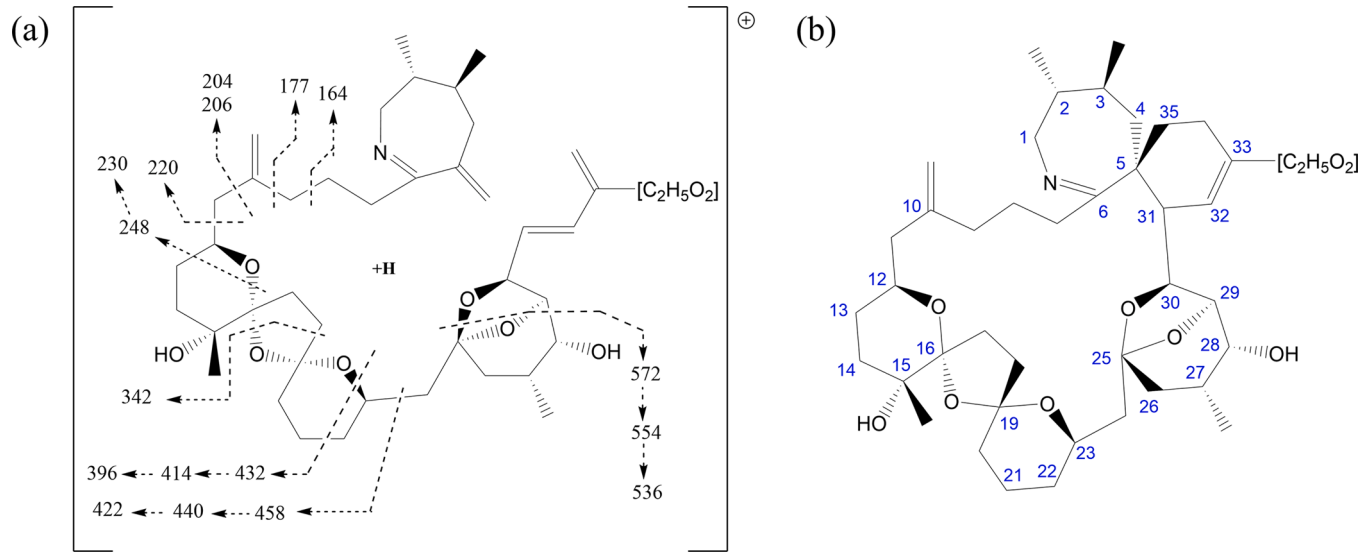

Fig. 10. Proposed fragmentation pattern of the protonated PnTX analog at *m/z* 728.4738, $[C_{42}H_{66}NO_9]^+$, after retro Diels-Alder reaction (a), and putative structure of this new analog of PnTX $C_{42}H_{65}NO_9$ (b).

Table 3
Indirect quantification of the unknown PnTX analog using the calibration curve of PnTX-G in mussels collected over 2018 in Ingril lagoon, France.

Sample	Sampling month	Unknown PnTX analog concentrations (µg/kg)	
		Non-hydrolyzed extract	Hydrolyzed extract
18 BM 012	January	1.9	3.3
18 BM 026	February	1.1	2.3
18 BM 042	March	1.2	2.0
18 BM 065	April	0.8	1.6
18 BM 107	May	0.9	1.6
18 BM 122	June	2.4	3.2
18 BM 150	July	3.4	3.4
18 BM 161	August	4.5	8.9
18 BM 194	September	1.9	3.0
18 BM 257	October	2.5	3.7
18 BM 271	November	0.6	1.0
18 BM 286	December	0.4	0.7

with 7-*O*-acyl-derivatives of dinophysistoxin-1, but free of okadaic acid or dinophysistoxin-1 (García et al., 2005).

The workflow dedicated to the study of biotransformation also allowed for the identification of a compound with its MS/MS spectrum presenting strong similarities with the known analogs of PnTXs. This compound did not correspond to any of the known PnTX analogs, and did not match compounds reported in the Comprehensive Marine Natural Products Database (Lyu et al., 2021), suggesting the discovery of a new PnTX analog. Given the available evidence, it was not possible to determine whether this analogue is directly produced by *V. rugosum* or if it results from the metabolism of a known pinnatoxin by the shellfish. The concentrations measured were lower than the PnTX-G levels measured in a previous study on the same samples, and of the same order of magnitude as PnTX-A levels (Hort et al., 2023). For instance, in the August mussels, the concentrations of PnTX-G and PnTX-A were 367.3 and 6.3 µg/kg of whole flesh, respectively, while the concentration of the unknown analog was estimated to 4.5 µg/kg (quantified indirectly with the PnTX-G calibration curve). The in-depth study of the fragmentation patterns from high-resolution MS/MS spectra enabled the proposal of a structure for this compound. Nevertheless, it was not possible to determine the atom arrangement $C_2H_5O_2$ for the side chain at C33, hindering the full elucidation of the structure of the unknown PnTX analog. The limitations of the available sample quantity and the low concentrations measured precluded the use of techniques such as nuclear magnetic resonance. The implementation of chemical and enzymatic conversions could be considered as interesting approaches to achieve this goal.

5. Conclusion

This study led to the discovery of a series of 13-*O*-acyl esters of portimine-A ($n = 13$), likely resulting from shellfish metabolism, as well as a new analog of PnTXs: $C_{42}H_{65}NO_9$. LC-MS/MS and LC-MS/HRMS instruments clearly demonstrated their complementarity. Untargeted acquisitions through high-resolution mass spectrometry made it possible to identify the first portimine-A ester (C16:0-portimine-A) and a putative unknown PnTX analog using the molecular networking approach, but also by screening a high number of possible transformations of known *V. rugosum* metabolites. In-depth investigations using triple quadrupole mass spectrometry enabled the detection of a higher number of portimine-A esters present at trace levels, owing to the high sensitivity of this type of analyzer. Additional investigations enabled the confirmation of the discovery of these compounds and the collection of structural information, essential to establish their full structure.

The fatty acid conjugation of portimine-A had not been reported previously. Nevertheless, its existence is not surprising as such conjugations have already been reported for a variety of other marine biotoxins in shellfish. Since fatty acid conjugated forms of marine toxins are generally released into the gastrointestinal tract during human digestion, it appears essential to monitor these analogs, at least indirectly, by implementing extract hydrolysis before analysis. In the present work, mussels were the only species of bivalve mollusk studied. It could be interesting to explore the toxin profiles of other species. The new analog of PnTXs was identified based on the MS/MS spectra similarities with PnTXs. Further studies are required to determine whether this compound is directly produced by *V. rugosum*, or results from shellfish metabolism. Moreover, the atom arrangement of the $C_2H_5O_2$ for the side chain at C33 still needs to be confirmed and fully elucidated.

This work contributes to improving our knowledge of the chemodiversity of the metabolites produced by *V. rugosum* or biotransformed in shellfish to better assess the risk to humans of exposure to these emerging toxins.

Funding

This research did not receive any specific grant from funding

agencies in the public, commercial, or not-for-profit sectors.

CRediT authorship contribution statement

Vincent Hort: Conceptualization, Data curation, Formal analysis, Investigation, Methodology, Project administration, Resources, Software, Supervision, Validation, Visualization, Writing – original draft, Writing – review & editing. **Sophie Bourcier:** Data curation, Formal analysis, Methodology, Writing – original draft, Writing – review & editing.

Declaration of competing interest

The authors declare that they have no known competing financial interests or personal relationships that could have appeared to influence the work reported in this paper.

Data availability

Data will be made available on request.

Acknowledgements

The authors sincerely acknowledge the Directorate General for Food (DGAl - French Ministry of Agriculture and Food), as pilot of the French program for monitoring emerging toxins (EMERGTOX scheme), and IFREMER, as coordinator of this program, for the collection of samples. We would also like to express our gratitude to Agnès Le Corre and Marie-Pierre Pavageau from Thermo Scientific for their valuable advice in the use of Compound Discoverer™ software.

Supplementary materials

Supplementary material associated with this article can be found, in the online version, at doi:10.1016/j.hal.2024.102621.

References

Aasen, J.A.B., Hardstaff, W., Aune, T., Quilliam, M.A., 2006. Discovery of fatty acid ester metabolites of spirolide toxins in mussels from Norway using liquid chromatography/tandem mass spectrometry. Rapid Commun. Mass Spectrom. 20, 1531–1537. https://doi.org/10.1002/rcm.2501.

Aráoz, R., Barnes, P., Séchet, V., Delepierre, M., Zinn-Justin, S., Molgó, J., Zakarian, A., Hess, P., Servent, D., 2020. Cyclic imine toxins survey in coastal european shellfish samples: bioaccumulation and mode of action of 28-O-palmitoyl ester of pinnatoxin-G. first report of portimine-A bioaccumulation. Harmful Algae 98, 101887. https://doi.org/10.1016/j.hal.2020.101887.

Arnich, N., Abadie, E., Delcourt, N., Fessard, V., Fremy, J.M., Hort, V., Lagrange, E., Maignien, T., Molgó, J., Peyrat, M.B., Vernoux, J.P., Mattei, C., 2020. Health risk assessment related to pinnatoxins in French shellfish. Toxicon 180, 1–10. https://doi.org/10.1016/j.toxicon.2020.03.007.

Braga, A.C., Alves, R.N., Maulvault, A.L., Barbosa, V., Marques, A., Costa, P.R., 2016. In vitro bioaccessibility of the marine biotoxin okadaic acid in shellfish. Food Chem. Toxicol. 89, 54–59. https://doi.org/10.1016/j.fct.2016.01.008.

Chou, T., Haino, T., Kuramoto, M., Uemura, D., 1996a. Isolation and structure of pinnatoxin D, a new shellfish poison from the okinawan bivalve Pinna muricata. Tetrahedron Lett 37, 4027–4030. https://doi.org/10.1016/0040-4039(96)00753-8.

Chou, T., Osamu, K., Uemura, D., 1996b. Relative stereochemistry of pinnatoxin A, a potent shellfish poison from Pinna muricata. Tetrahedron Lett. 37, 4023–4026. https://doi.org/10.1016/0040-4039(96)00752-6.

Clarke, M.R., Jones, B., Squires, C.L.M., Imhoff, F.M., Harwood, D.T., Rhodes, L., Selwood, A.I., McNabb, P.S., Baird, S.K., 2021. Cyclic imine pinnatoxin g is cytotoxic to cancer cell lines via nicotinic acetylcholine receptor-driven classical apoptosis. J. Nat. Prod. 84, 2035–2042. https://doi.org/10.1021/acs.jnatprod.1c00418.

De la Iglesia, P., McCarron, P., Diogène, J., Quilliam, M.A., 2013. Discovery of gymnodimine fatty acid ester metabolites in shellfish using liquid chromatography/mass spectrometry. Rapid Commun. Mass Spectrom. 27, 643–653. https://doi.org/10.1002/rcm.6491.

Dernekbasi, S., Oksuz, A., Celik, M.Y., Karay, I., Karay, S., 2015. The fatty acid composition of cultured mussels (mytilus galloprovincialis lamarck 1819) in offshore longline system in the black sea. J. Aquac. Mar. Biol. Volume 2. https://doi.org/10.15406/jamb.2015.02.00049.

EFSA Panel on Contaminants in the Food Chain (CONTAM), 2010. Scientific Opinion on marine biotoxins in shellfish – Cyclic imines (spirolides, gymnodimines, pinnatoxins and pteriatoxins). EFSA J. 8, 1628. https://doi.org/10.2903/j.efsa.2010.1628.

Fribley, A.M., Xi, Y., Makris, C., Alves-de-Souza, C., York, R., Tomas, C., Wright, J.L.C., Strangman, W.K., 2019. Identification of Portimine B, a New Cell Permeable Spiroimine That Induces Apoptosis in Oral Squamous Cell Carcinoma. ACS Med. Chem. Lett. 10, 175–179. https://doi.org/10.1021/acsmedchemlett.8b00473.

García, C., Truan, D., Lagos, M., Santelices, J.P., Díaz, J.C., Lagos, N., 2005. Metabolic transformation of dinophysistoxin-3 into dinophysistoxin-1 causes human intoxication by consumption of O-acyl-derivatives dinophysistoxins contaminated shellfish. J. Toxicol. Sci. 30, 287–296. https://doi.org/10.2131/jts.30.287.

García-Altares, M., Casanova, A., Bane, V., Diogène, J., Furey, A., de la Iglesia, P., 2014. Confirmation of pinnatoxins and spirolides in shellfish and passive samplers from catalonia (Spain) by liquid chromatography coupled with triple quadrupole and high-resolution hybrid tandem mass spectrometry. Mar. Drugs 12, 3706–3732. https://doi.org/10.3390/md12063706.

Hampton, M.B., Selwood, A.I., Shi, F., 2014. Bioactive compounds. WO2014/189393.

Hermawan, I., Higa, M., Hutabarat, P.U.B., Fujiwara, T., Akiyama, K., Kanamoto, A., Haruyama, T., Kobayashi, N., Higashi, M., Suda, S., Tanaka, J., 2019. Kabirimine, a New Cyclic Imine from an Okinawan Dinoflagellate. Mar. Drugs 17, 353. https://doi.org/10.3390/md17060353.

Hess, P., Abadie, E., Hervé, F., Berteaux, T., Séchet, V., Aráoz, R., Molgó, J., Zakarian, A., Sibat, M., Rundberget, T., Miles, C.O., Amzil, Z., 2013. Pinnatoxin G is responsible for atypical toxicity in mussels (Mytilus galloprovincialis) and clams (Venerupis decussata) from Ingril, a French Mediterranean lagoon. Toxicon 75, 16–26. https://doi.org/10.1016/j.toxicon.2013.05.001.

Hess, P., Mertens, K., Chomerat, N., Sechet, V., Herve, F., Plessis, L., Reveillon, D., Brehmer, P., 2022. Vulcanodinium rugosum - a potent and ubiquitous genus affecting mice and man. In: Presented at the Dinophyte Seminars. Université Louis-et-Maximilien en ligne [2 p.].

Hort, V., Bastardo-Fernández, I., Nicolas, M., 2023. Exploration of Vulcanodinium rugosum Toxins and their Metabolism Products in Mussels from the Ingril Lagoon Hotspot in France. Mar. Drugs 21, 429. https://doi.org/10.3390/md21080429.

Lamas, J.P., Arévalo, F., Moroño, Á., Correa, J., Muñíz, S., Blanco, J., 2019. Detection and spatio-temporal distribution of pinnatoxins in shellfish from the atlantic and cantabrian coasts of Spain. Toxins (Basel) 11, 340. https://doi.org/10.3390/toxins11060340.

Lyu, C., Chen, T., Qiang, B., Liu, N., Wang, H., Zhang, L., Liu, Z., 2021. CMNPD: a comprehensive marine natural products database towards facilitating drug discovery from the ocean. Nucleic Acids Res 49, D509–D515. https://doi.org/10.1093/nar/gkaa763.

Manita, D., Alves, R.N., Braga, A.C., Fogaça, F.H.S., Marques, A., Costa, P.R., 2017. In vitro bioaccessibility of the marine biotoxins okadaic acid, dinophysistoxin-2 and their 7-O-acyl fatty acid ester derivatives in raw and steamed shellfish. Food Chem. Toxicol. 101, 121–127. https://doi.org/10.1016/j.fct.2017.01.008.

Marr, J.C., Hu, T., Pleasance, S., Quilliam, M.A., Wright, J.L.C., 1992. Detection of new 7-O-acyl derivatives of diarrhetic shellfish poisoning toxins by liquid chromatography-mass spectrometry. Toxicon 30, 1621–1630. https://doi.org/10.1016/0041-0101(92)90034-3.

McCarron, P., Rourke, W.A., Hardstaff, W., Pooley, B., Quilliam, M.A., 2012. Identification of pinnatoxins and discovery of their fatty acid ester metabolites in mussels (mytilus edulis) from eastern canada. J. Agric. Food Chem. 60, 1437–1446. https://doi.org/10.1021/jf204824s.

McNabb, P.S., McCoubrey, D.J., Rhodes, L., Smith, K., Selwood, A.I., van Ginkel, R., MacKenzie, A.L., Munday, R., Holland, P.T., 2012. New perspectives on biotoxin detection in Rangaunu Harbour, New Zealand arising from the discovery of pinnatoxins. Harmful Algae 13, 34–39. https://doi.org/10.1016/j.hal.2011.09.013.

Mondeguer, F., Abadie, E., Herve, F., Bardouil, M., Sechet, V., Raimbault, V., Berteaux, T., Zendong, S.Z., Palvadeau, H., Amzil, Z., Hess, P., Fessard, V., Huguet, A., Sosa, S., Tubaro, A., Aráoz, R., Molgó, J., 2015. Pinnatoxines en lien avec l'espèce Vulcanodinium rugosum (II).

Moreira-González, A.R., Comas-González, A., Valle-Pombrol, A., Seisdedo-Losa, M., Hernández-Leyva, O., Fernandes, L.F., Chomérat, N., Bilien, G., Hervé, F., Rovillon, G.A., Hess, P., Alonso-Hernández, C.M., Mafra, L.L., 2020. Summer bloom of Vulcanodinium rugosum in Cienfuegos Bay (Cuba) associated to dermatitis in swimmers. Sci. Total Environ., 143782 https://doi.org/10.1016/j.scitotenv.2020.143782.

Mudge, E.M., Miles, C.O., Hardstaff, W.R., McCarron, P., 2020. Fatty acid esters of azaspiracids identified in mussels (Mytilus edulis) using liquid chromatography-high resolution mass spectrometry. Toxicon X 8. https://doi.org/10.1016/j.toxcx.2020.100059.

Munday, R., Selwood, A.I., Rhodes, L., 2012. Acute toxicity of pinnatoxins E, F and G to mice. Toxicon 60, 995–999. https://doi.org/10.1016/j.toxicon.2012.07.002.

Nézan, E., Chomérat, N., 2011. *Vulcanodinium rugosum* gen. et sp. nov. (Dinophyceae), un Nouveau Dinoflagellé Marin de la Côte Méditerranéenne Française. Cryptogam. Algol. 32, 3–18. https://doi.org/10.7872/crya.v32.iss1.2011.003.

Norambuena, L., Mardones, J.I., 2023. Emerging phycotoxins in the Chilean coast: first localized detection of the neurotoxic cyclic imine Pinnatoxin-G in shellfish banks. Mar. Pollut. Bull. 190, 114878 https://doi.org/10.1016/j.marpolbul.2023.114878.

Pan, W., Ji, Y., Qiu, J., Wang, G., Tang, Z., Li, A., 2022. Comparative study on the esterification of gymnodimine in different shellfish exposed to the dissolved toxin in seawater. Harmful Algae 115, 102233. https://doi.org/10.1016/j.hal.2022.102233.

R Core Team, 2016. R: A Language and Environment for Statistical Computing. R Foundation for Statistical Computing, Vienna, Austria.

Rambla-Alegre, M., 2018. occurrence of cyclic imines in european commercial seafood and consumers risk assessment. Environ. Res. 7.

Rundberget, T., Aasen, J.A.B., Selwood, A.I., Miles, C.O., 2011. Pinnatoxins and spirolides in Norwegian blue mussels and seawater. Toxicon 58, 700–711. https://doi.org/10.1016/j.toxicon.2011.08.008.

Selwood, A.I., Miles, C.O., Wilkins, A.L., van Ginkel, R., Munday, R., Rise, F., McNabb, P., 2010. Isolation, structural determination and acute toxicity of pinnatoxins E, F and G. J. Agric. Food Chem. 58, 6532–6542. https://doi.org/10.1021/jf100267a.

Selwood, A.I., Wilkins, A.L., Munday, R., Gu, H., Smith, K.F., Rhodes, L.L., Rise, F., 2014. Pinnatoxin H: a new pinnatoxin analogue from a South China Sea Vulcanodinium rugosum isolate. Tetrahedron Lett 55, 5508–5510. https://doi.org/10.1016/j.tetlet.2014.08.056.

Selwood, A.I., Wilkins, Munday, Shi, Rhodes, 2013. Portimine: a bioactive metabolite from the benthic dinoflagellate Vulcanodinium rugosum. Tetrahedron Lett. 3.

Sievert, C., 2020. Interactive Web-Based Data Visualization with R, plotly, and Shiny. Chapman and Hall/CRC.

Sosa, S., Pelin, M., Cavion, F., Hervé, F., Hess, P., Tubaro, A., 2020. Acute oral toxicity of pinnatoxin G in mice. Toxins (Basel) 12, 87. https://doi.org/10.3390/toxins12020087.

Takada, N., Umemura, N., Suenaga, K., Chou, T., Nagatsu, A., Haino, T., Yamada, K., Uemura, D., 2001a. Pinnatoxins B and C, the most toxic components in the pinnatoxin series from the Okinawan bivalve Pinna muricata. Tetrahedron Lett. 42, 3491–3494. https://doi.org/10.1016/S0040-4039(01)00480-4.

Takada, N., Umemura, N., Suenaga, K., Uemura, D., 2001b. Structural determination of pteriatoxins A, B and C, extremely potent toxins from the bivalve Pteria penguin. Tetrahedron Lett. 42, 3495–3497. https://doi.org/10.1016/S0040-4039(01)00478-6.

Tamele, I.J., Timba, I., Vasconcelos, V., Costa, P.R., 2022. First report of pinnatoxins in bivalve molluscs from inhaca island (south of mozambique)—south of the indian ocean. J. Mar. Sci. Eng. 10, 1215. https://doi.org/10.3390/jmse10091215.

Uemura, D., Chou, T., Haino, T., Nagatsu, A., Fukuzawa, S., Zheng, S., Chen, H., 1995. Pinnatoxin A: a toxic amphoteric macrocycle from the Okinawan bivalve Pinna muricata. J. Am. Chem. Soc. 117, 1155–1156. https://doi.org/10.1021/ja00108a043.

Yanagi, T., Murata, M., Torigoe, K., Yasumoto, T., 1989. Biological activities of semisynthetic analogs of dinophysistoxin-3, the major diarrhetic shellfish toxin. Agric. Biol. Chem. 53, 525–529. https://doi.org/10.1080/00021369.1989.10869308.

Zheng, S., Huang, F., Chen, S., Tan, X., Zuo, J., Peng, J., Xie, R., 1990. The isolation and bioactivities of pinnatoxin. Chin. J. Mar. Drugs 9, 33–35.